Physics Letters B 811 (2020) 135942

Contents lists available at ScienceDirect

Physics Letters B

www.elsevier.com/locate/physletb

Scattering of the halo nucleus ^{11}Be from a lead target at 3.5 times the Coulomb barrier energy

RIBLL Collaboration

F.F. Duan [a,b,1], Y.Y. Yang [a,c,*,1], K. Wang [a], A.M. Moro [d,e,*], V. Guimarães [f], D.Y. Pang [g], J.S. Wang [h,a,c], Z.Y. Sun [a,c], Jin Lei [a,2], A. Di Pietro [i], X. Liu [j], G. Yang [a,c], J.B. Ma [a,c], P. Ma [a], S.W. Xu [a], Z. Bai [a], X.X. Sun [b], Q. Hu [a], J.L. Lou [k], X.X. Xu [a,c], H.X. Li [a], S.Y. Jin [a], H.J. Ong [a], Q. Liu [l], J.S. Yao [h], H.K. Qi [h], C.J. Lin [m], H.M. Jia [m], N.R. Ma [m], L.J. Sun [m,n], D.X. Wang [m], Y.H. Zhang [a,c], X.H. Zhou [a,c], Z.G. Hu [a,c], H.S. Xu [a,c]

[a] CAS Key Laboratory of High Precision Nuclear Spectroscopy, Institute of Modern Physics, Chinese Academy of Sciences, Lanzhou 730000, China
[b] School of Nuclear Science and Technology, Lanzhou University, Lanzhou 730000, China
[c] School of Nuclear Science and Technology, University of Chinese Academy of Sciences, Beijing 100080, China
[d] Departamento de FAMN, Universidad de Sevilla, Apartado 1065, 41080 Sevilla, Spain
[e] Instituto Interuniversitario Carlos I de Física Teórica y Computacional (iC1), Apdo. 1065, E-41080 Sevilla, Spain
[f] Instituto de Física, Universidade de São Paulo, Rua do Matão, 1371, São Paulo 05508-090, SP, Brazil
[g] School of Physics, Beijing Key Laboratory of Advanced Nuclear Materials and Physics, Beihang University, Beijing, 100191, China
[h] School of Science, Huzhou University, Huzhou 313000, China
[i] INFN-Laboratori Nazionali del Sud, Via S. Sofia 62, I-95123 Catania, Italy
[j] Key Laboratory of Radiation Physics and Technology of the Ministry of Education, Institute of Nuclear Science and Technology, Sichuan University, Chengdu 610064, China
[k] School of Physics, State Key Laboratory of Nuclear Physics and Technology, Peking University, Beijing 100871, China
[l] School of Physics and Materials Science, Anhui University, Hefei 230601, China
[m] Department of Nuclear Physics, China Institute of Atomic Energy, Beijing 102413, China
[n] School of Physics and Astronomy, Shanghai Jiao Tong University, Shanghai 200240, China

ARTICLE INFO

Article history:
Received 20 June 2020
Received in revised form 4 November 2020
Accepted 5 November 2020
Available online 11 November 2020
Editor: D.F. Geesaman

Keywords:
Elastic scattering
Breakup reaction
Breakup coupling effects
CDCC
XCDCC

ABSTRACT

Angular distributions of quasielastic scattering and breakup of the neutron-rich halo nucleus ^{11}Be on a ^{208}Pb target at an incident energy of 140 MeV (about 3.5 times the Coulomb barrier) were measured at HIRFL-RIBLL. A strong suppression of the Coulomb nuclear interference peak is observed in the measured quasielastic scattering angular distribution. The result demonstrates for the first time the persistence of the strong breakup coupling effect reported so far for reaction systems involving neutron-halo nuclei at this relatively high incident energy. The measured quasielastic scattering cross sections are satisfactorily reproduced by continuum discretized coupled channel (CDCC) calculations as well as by the XCDCC calculations where the deformation of the ^{10}Be core is taken into account. The angular and energy distributions of the ^{10}Be fragments could also be well reproduced considering elastic breakup (CDCC and XCDCC) plus nonelastic breakup contributions, with the latter evaluated with the model by Ichimura, Austern and Vincent [1]. The comparison of the ^{10}Be energy distributions with simple kinematical estimates evidence the presence of a significant post-acceleration effect which, in the (X)CDCC frameworks, is accounted for by continuum-continuum couplings.

1. Introduction

Elastic and breakup reactions induced by stable as well as unstable atomic nuclei constitute a fruitful area of research in nuclear physics. The angular distributions of elastic scattering cross sections can exhibit different features depending on the incident energy and on the structure of the colliding nuclei. For ordinary

* Corresponding authors.
E-mail addresses: yangyanyun@impcas.ac.cn (Y.Y. Yang), moro@us.es (A.M. Moro).
[1] These authors contributed equally to this work and should be considered co-first authors.
[2] Current address: Istituto Nazionale di Fisica Nucleare, Sezione di Pisa, Largo Pontecorvo 3, 56127 Pisa, Italy.

https://doi.org/10.1016/j.physletb.2020.135942

projectiles, and at energies close to the Coulomb barrier, a typical Fresnel oscillatory diffraction pattern may appear when the angular distribution is plotted as the ratio to the Rutherford scattering cross sections. This Fresnel peak, usually called the Coulomb-nuclear interference peak (CNIP) or Coulomb rainbow, is due to the interference between partial waves refracted by the Coulomb and short-range nuclear potentials. For light projectiles, the Coulomb force becomes smaller and the diffractive pattern changes from Fresnel to Fraunhofer oscillations at higher energies [2]. While stable and ordinary tightly bound nuclei exhibit one or the other of these classical diffraction patterns in their angular distributions, a clear deviation from the oscillatory pattern is observed for the elastic scattering induced by weakly-bound nuclei. These nuclei are characterized by low binding energies of the valence particle(s) with respect to the core, giving rise to some decoupling during the collision. This effect leads to the appearance of non-elastic processes, even at large distances, producing a damping or completely disappearance of the Fresnel peak.

^{11}Be is an archetype of one-neutron halo nucleus [3,4]. Its valence neutron has a low binding energy, $S_n = 0.503$ MeV, in the ground state and 0.181 MeV in the first excited state. The ground state of ^{11}Be is known to consist of an admixture of s- and d-wave neutron configurations, with the latter associated with the excitation of the ^{10}Be core [5,6]. Measurements of the elastic scattering of ^{11}Be have been made at energies around the Coulomb barrier on several medium to heavy targets, namely, ^{64}Zn [7,8], ^{120}Sn [9], ^{197}Au [10], and ^{209}Bi [11,12]. The angular distributions in all these experiments exhibit a strong suppression of the CNIP due to strong breakup coupling effects. Strong damping of the CNIP has also been observed in the elastic scattering of other weakly-bound neutron rich nuclei, such as ^{6}He [13–17] and ^{11}Li [18] on heavy targets, but also at energies close to the barriers.

Elastic scattering measurements of proton-rich nuclei, such as ^{8}B, ^{9}C, ^{10}C, and ^{17}F have been performed on ^{58}Ni and ^{208}Pb targets [19–27]. The ^{8}B nucleus has a very weakly bound valence proton with separation energy $S_p = 0.1375$ MeV, and no bound excited states. Angular distributions for the elastic scattering of the ^{8}B + ^{58}Ni system were measured at several energies close to the Coulomb barrier [19]. The CDCC calculations for this data set indicated a strong influence of the breakup channel, although the CNIP is not apparent in the angular distributions [28,29]. More recently, a calculation based on a microscopic version of the CDCC method, MCDCC, has been performed, predicting the existence of CNIP for this system [30]. In spite of such differences, both calculations suggested that the breakup coupling effects to the elastic scattering angular distributions are small for the ^{8}B + ^{58}Ni system at around Coulomb barrier energies.

The breakup effect on the elastic scattering could be better investigated with heavier targets due to the increasing predominance of the long-range Coulomb interaction compared to the nuclear potential. Two measurements have been performed for the ^{8}B + ^{208}Pb system: one at an energy close to the coulomb barrier ($E_{\rm Lab} = 50$ MeV) [20] and another at three times the Coulomb barrier energy ($E_{\rm Lab} = 170$ MeV) [21]. Full CDCC calculations performed for this system reasonably reproduced the corresponding experimental angular distributions. The same has been found for MCDCC calculation from Ref. [30]. The conclusion is that for this system, the breakup effects on the elastic scattering angular distributions are not so strong compared to what is found for weakly-bound neutron-rich nuclei. Similar conclusions have been found in elastic scattering of other proton-rich nuclei such as ^{9}C [23] and ^{17}F [24–27].

Understanding the interplay between the nuclear structure and reaction mechanism and the influence of the breakup coupling effects in the elastic and fusion processes is still a challenge for both theoretical and experimental studies. Calculations performed by Yang, Liu and Pang [31] have shown that the Coulomb and centrifugal barriers, experienced by the valence proton in the ground state of ^{8}B but absent for the valence neutron in the ground state of ^{11}Be, are responsible for the distinct difference in the elastic scattering angular distributions of these two typical weakly bound nuclei. It has been commonly believed that multistep effects, such as those appearing in inelastic excitation, get smaller at high incident energies, due to the smaller collision time. Consequently, one may argue that the seemingly weak breakup coupling effects observed in the elastic scattering angular distributions of proton-rich nuclei may be attributed to the fact that they were measured at too high incident energies. It is interesting to see how the elastic scattering angular distributions would be affected by the breakup channels for weakly bound neutron rich nuclei at such incident energies. So far, measurements of the elastic scattering and breakup cross sections with heavy targets for weakly-bound neutron rich nuclei were all performed at energies around the Coulomb barrier. To contribute to the discussions described above, this paper reports, for the first time, measurement of the elastic scattering and breakup reactions of ^{11}Be on ^{208}Pb at an incident energy of 140 MeV, which corresponds to about 3.5 times of the Coulomb barrier ($V_B \approx 39.5$ MeV). Elastic scattering of ^{9}Be and ^{10}Be + ^{208}Pb were simultaneously measured in the present experiment, which are important for the completion of the theoretical analysis of the ^{11}Be data.

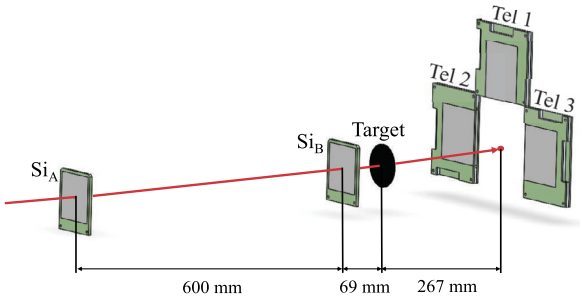

Fig. 1. Schematic view of the experimental setup.

2. Experiment and data analyses

The experiment was performed at the Radioactive Ion Beam Line in Lanzhou [32], the Heavy Ion Research Facility of Lanzhou [33] (HIRFL-RIBLL). The secondary ^{9}Be, ^{10}Be, and ^{11}Be beams were produced by the fragmentation of a primary ^{13}C beam, delivered by the HIRFL on a 4500 μm Be target at 54.2 MeV/nucleon. The beam energies at the center of the reaction target were 88, 127 and 140 MeV for ^{9}Be, ^{10}Be, and ^{11}Be, respectively. The secondary beams were identified using the time-of-flight (ToF) measurement between two 50 μm thick plastic scintillators 1680 cm apart (flight length). The beam intensities of ^{9}Be, ^{10}Be, and ^{11}Be were 7×10^3, 6×10^3 and 2×10^3 particles per second, respectively. The ^{208}Pb target is a self-supporting foil with a thickness of 8.52 mg/cm^2. The schematic view of the detector setup is shown in Fig. 1. Two double-sided silicon strip detectors (DSSD), SiA and SiB, are positioned at 669 mm and 69 mm away from the target position, respectively. Their thicknesses are 74 and 87 μm, respectively, and both have 16 horizontal and 16 vertical strips. The tracks of the incoming particles were determined by SiA and SiB and were extrapolated to the target position event by event. An array of three $\Delta E - E$ particle telescopes, named Tel1, Tel2, and Tel3, were used to detect the scattered particles. Each of these telescopes consisted of a DSSD and a single-sided detector (SSD), covering a range of scattering angles from 5° to 27° in the laboratory system. The detector array assembly was mounted 267 mm downstream the target.

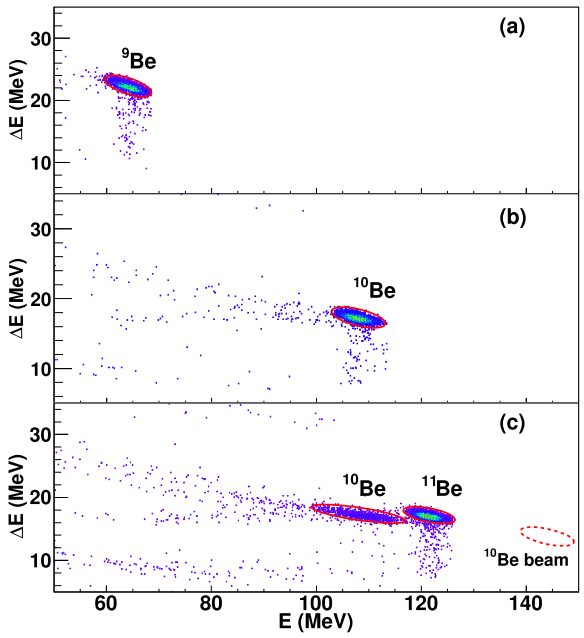

Fig. 2. The two-dimensional $\Delta E - E$ particle identification spectra for the (a) ^{9}Be, (b) ^{10}Be and (c) ^{11}Be beams within all the angles covered by the current measurement. In (c), the expected loci of ^{10}Be beam contamination are indicated and it is well separated from the group of ^{10}Be breakup fragment particles.

The DSSDs in these telescopes consisted of 32 strips on each side with 64×64 mm^2 of total active areas, and are 301, 129, and 144 μm thick for Tel1, Tel2, and Tel3, respectively. They allowed us to determine the positions of the scattered particles accurately within areas of 2×2 mm^2. The SSD detectors, which provided the E signals of the scattered particles, have thicknesses of 1536, 1535, and 1528 μm, respectively and have the same effective areas as the DSSDs.

Typical two-dimensional $\Delta E - E$ particle identification spectra for the ^{9}Be, ^{10}Be, and ^{11}Be beams are shown in Fig. 2 (a), (b) and (c). Only elastic scattering events were observed for the ^{9}Be and ^{10}Be beams, while for the ^{11}Be beam, both ^{11}Be and ^{10}Be particles were observed. The latter being produced by the interaction of ^{11}Be with the target (projectile breakup and/or transfer). As seen in Fig. 2 (c), our telescopes can clearly distinguish the reaction products, ^{10}Be, from the elastically scattered ^{11}Be particles. This clear particle identification has been achieved within all the angles covered by our measurement. The purity of the ^{11}Be beam is higher than 82%. The main contaminations are ^{10}Be and ^{12}B particles. The ^{10}Be particles as reaction products can be well separated from the elastic scattering events induced by the beam contaminant ^{10}Be, which centered at around 158 MeV (red-dotted gate) in the $\Delta E - E$ spectrum.

A Monte Carlo simulation was used to evaluate the absolute differential cross sections. Assuming pure Rutherford scattering at all angles, taking into account the actual geometry of detector setup and the beam track measured by SiA and SiB, one can obtain the Rutherford scattering yield $N(\theta)_{Ruth}$ at a given θ. The elastic scattering differential cross section $d\sigma(\theta)_{exp}$ as the ratio to the Rutherford cross section $d\sigma(\theta)_{Ruth}$ is obtained by: $\frac{d\sigma_{exp}(\theta)}{d\sigma_{Ruth}(\theta)} = C \times \frac{N(\theta)_{exp}}{N(\theta)_{Ruth}}$. The overall normalization factor was obtained by normalizing the cross sections measured at angles smaller than 20° for the ^{9}Be elastic scattering to the Rutherford cross sections. At these small angles the cross sections are assumed to be pure Rutherford. The resulting normalization factor was, then, used to normalize the elastic scattering cross sections for ^{10}Be and ^{11}Be. In order to minimize the systematic errors, small corrections for detector misalignment were also applied. Details of the data analysis can be found in Refs. [34,35].

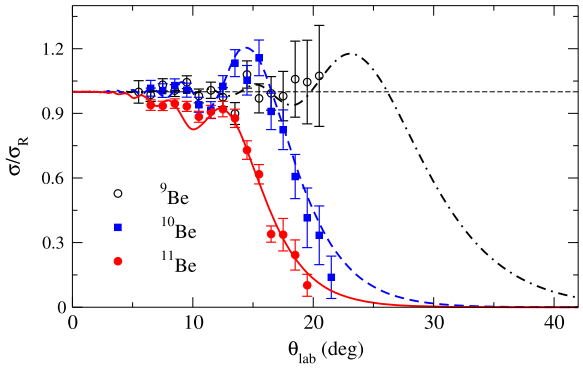

Fig. 3. Quasielastic scattering angular distributions for ^{9,10,11}Be + ^{208}Pb. The dash-dotted, dashed and solid curves are results of optical model calculations for ^{9}Be, ^{10}Be, and ^{11}Be, respectively. See the text for details.

The experimental angular distributions for the elastic scattering of ^{9}Be, ^{10}Be and ^{11}Be projectiles on a ^{208}Pb target are shown in Fig. 3 as ratios to the corresponding Rutherford cross sections. The error bars are for statistical errors only. The angular distributions were obtained with an interval of 1° in the laboratory frame. Due to the energy dispersion of the secondary beams and the intrinsic energy resolution of our detectors, it was not possible to separate the inelastic events from the elastic ones. These data are thus quasielastic in nature. Contributions from the excitation of the lead target are assumed to be negligible, as that has been made at several other experiments at similar incident energies [21–23]. The contribution from the excitation of the first excited state of ^{11}Be can be estimated in CDCC/XCDCC calculations, which will be shown in the following section. The ^{10}Be particles downstream of the target in Fig. 2 (c) may be products of either breakup or neutron transfer reactions. However, cross sections of latter have been estimated to be negligible at the present incident energy, so these events are taken inclusively as the product of the projectile breakup reaction.

3. Results and discussions

Comparisons between the angular distributions of the measured quasielastic scattering cross sections of ^{9}Be, ^{10}Be, and ^{11}Be from the lead target and the elastic scattering cross sections from optical model calculations are depicted in Fig. 3. The systematic folding model nucleus-nucleus potential of Ref. [36] is used for ^{9}Be and ^{10}Be. Result of optical model calculation suggests that the quarter-point angle for the ^{9}Be + ^{208}Pb system is about 35°, which is much larger than the covered angular range in our experiment. At scattering angles smaller than 20°, the measured ratio-to-Rutherford cross sections are very close to unity, which justifies our use of this set of data to make overall normalizations in our experiment. The angular distribution of ^{10}Be + ^{208}Pb system shows a typical CNIP, as expected for a tightly-bound nucleus. The systematic potential accounts for these data reasonably well, as shown by the blue dashed curve. The angular distribution of the ^{11}Be + ^{208}Pb system, on other hand, shows a strong damping of the CNIP, which can not be accounted for by the systematic potential. The discrepancy is attributed to the presence of long-range absorption effects, mostly arising from the strong dipole Coulomb breakup mechanism. This effect can be accommodated in the OM framework in the form of a polarization potential. In the present analysis, we have adopted the dynamic dipole polarization (DPP) potential of Refs. [37,38] (see also [39] for a recent application to ^{11}Be), which accounts for the effect of the coupling to the excited states on the elastic cross section due to second-order action

of the dipole Coulomb interaction. In the case of ^{11}Be scattering, the DPP contains contributions from both the $1/2^-$ bound excited state as well as from continuum states and, as such, requires as ingredient the $B(E1)$ connecting the ground state with all these states. In the present calculations these $B(E1)$ values have been computed with the particle-plus-rotor model (CEX) of Ref. [40]. This model, described below in more detail, accounts explicitly for the ^{10}Be deformation and produces a $dB(E1)/E$ distribution in good agreement with that extracted from the Coulomb dissociation experiment of Fukuda et al. [41]. Adding this DPP to the bare ^{10}Be + ^{208}Pb potential, we obtain a very good reproduction of the measured quasielastic data (solid curve). The total reaction cross sections from these OM calculations are $\sigma_R = 2473$, 3067, and 7798 mb, for ^{9}Be, ^{10}Be, and ^{11}Be, respectively. The extraordinary large σ_R value of the ^{11}Be + ^{208}Pb system is associated with the strong breakup channel arising from the special, weakly-bound structure of this nucleus.

To investigate the interplay of nuclear structure and reaction dynamics in the quasielastic scattering angular distributions, CDCC and XCDCC calculations have been performed for the ^{11}Be + ^{208}Pb system. The CDCC calculations employ a single-particle (SP) model of ^{11}Be, which ignores the structure of the ^{10}Be core. The relative motion between the halo neutron and the inert ^{10}Be core is described with the Woods-Saxon potential of Ref. [42], which reproduces the separation energy of the valence neutron in the ground and the first excited state of ^{11}Be as well as the position of the $5/2^+_1$ low-lying resonance. A binning procedure was used to describe the continuum states. Continuum states with maximum orbital angular momentum $\ell_{\max} = 6$ and excitation energy up to $\varepsilon_{\max} = 12$ MeV above the breakup threshold were included.

We have also performed extended CDCC (XCDCC) calculations, in which the effects of ^{10}Be deformation and excitation are explicitly taken into account. In the present XCDCC calculations, the ^{11}Be states are described using the aforementioned CEX particle-plus-rotor model of Ref. [40], which takes into account the ground state (0^+_1) and the first excited state (2^+_1) of the ^{10}Be core. The n-^{10}Be interaction contains central and spin-orbit terms with the usual Woods-Saxon volume and derivative shapes, respectively. Quadrupole couplings are also included by deforming the central part with a deformation parameter $\beta_2 = 0.67$ [43]. These couplings produce admixtures of the ^{10}Be(0^+_1) and ^{10}Be(2^+_1)states in the ^{11}Be states. For example, the resultant ground-state wave function has a 88% of ^{10}Be(0^+_1) $\otimes\, \nu s_{1/2}$ configuration.

The energies and wave functions of the ^{11}Be states are calculated with the pseudostate (PS) method [44], which consists in diagonalizing the Hamiltonian of this composite system in a convenient basis of square-integrable functions. In this work, we use the Transformed Harmonic Oscillator (THO) basis, which is obtained by application of a local scaled transformation (LST) to the conventional HO basis. In particular, we use the analytical LST proposed in Ref. [45], which has been already applied to ^{11}Be in Refs. [44,46], and the parameters used in the present calculations are similar to those employed in that reference. The size of the basis is determined by the number of oscillator functions (N), the maximum excitation energy ($\varepsilon_{\max}$), the maximum orbital angular momentum for the core-valence motion ($\ell_{\max}$), the maximum valence + core angular momentum ($j_{\max}$) and the number of the core states. In the present calculations we use $N = 10 - 20$ (depending on the partial wave), $\varepsilon_{\max} = 13$ MeV, $\ell_{\max} = 9$ and $j_{\max} = 13/2$.

In both the CDCC and XCDCC calculations the OMP parameters between the valence neutron and ^{208}Pb are taken from the systematic nucleon-nucleus OMP of Ref. [47]. The core-target OMP was obtained from the systematic nucleus-nucleus potential of Ref. [36], which, as shown in Fig. 3, reproduced the ^{10}Be + ^{208}Pb elastic scattering data reasonably well.

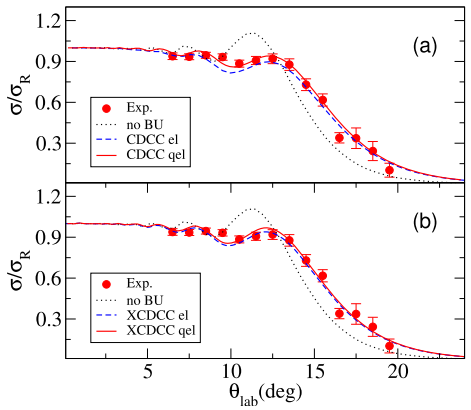

Fig. 4. Comparisons between results of CDCC (upper panel) and XCDCC (lower panel) calculations and the experimental data of the quasielastic scattering of ^{11}Be + ^{208}Pb at $E_{\rm lab} = 140$ MeV. The dashed and dotted curves are for elastic scattering with and without including the continuum-continuum couplings, respectively. The solid curves are for quasielastic scattering, which are sums of elastic and inelastic scattering cross sections.

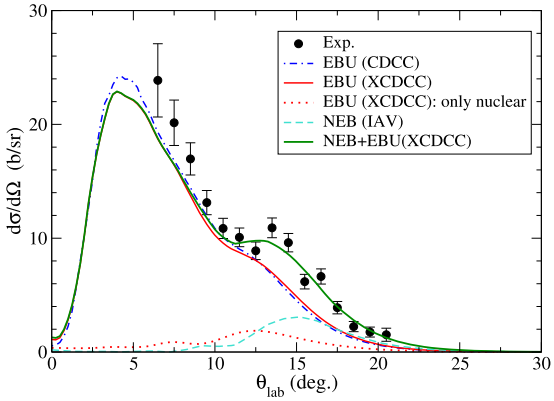

Fig. 5. Experimental differential breakup cross section for ^{11}Be + ^{208}Pb system at $E_{\rm lab} = 140$ MeV compared with the CDCC and XCDCC calculations, for the elastic breakup part, and IAV calculations, for the NEB part. See text for the details.

The results of these calculations are shown in Fig. 4 (a) and (b) for quasielastic scattering and in Figs. 5 and 6 for the breakup reaction. As we can see in Fig. 4, CDCC and XCDCC calculations reproduce the quasielastic scattering data nearly equally well. A closer inspection of Fig. 4 shows that, although the CDCC and XCDCC calculations produce similar quasielastic cross sections, they predict somewhat different elastic (and, consequently, inelastic) cross sections. As a result, the quasielastic scattering cross section, which is the sum of the elastic and inelastic cross sections, is rather close for CDCC and XCDCC. The same has been found for the ^{11}Be + ^{64}Zn [6] and ^{11}Be + ^{197}Au [10] reactions at near-barrier energies. As explained in [6], the difference in the predicted inelastic cross section is due to the rather different $B(E1; \text{g.s.} \rightarrow 1/2^-_1)$ values given by the SP and CEX models used, respectively, in the CDCC and XCDCC calculations. The importance of the breakup channels on the elastic scattering can be assessed by comparing the one-channel (no-BU) CDCC and XCDCC calculation, dotted line in Fig. 4, which corresponds to a calculation where all couplings to the continuum are switched off, with the full CDCC and XCDCC calculations. As can be seen in Fig. 4 (a) and (b), the full calculations reproduce the strong reduction of the CNIP, confirming that the strong breakup coupling effects, which has been mostly reported for halo nuclei at near-barrier energies, persist in the case of the ^{11}Be halo nucleus at incident energies several times higher than that of the Coulomb barrier.

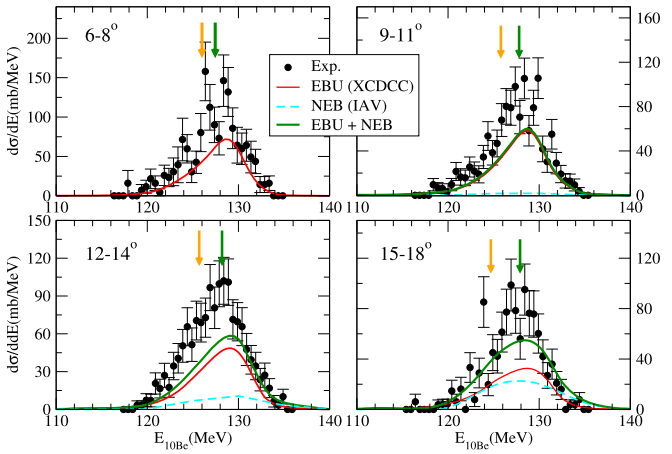

Fig. 6. Energy distributions of the breakup fragment ^{10}Be for the indicated angular intervals. The orange and green arrows correspond to the estimated ^{10}Be energies excluding and including post-acceleration, respectively (see text for details).

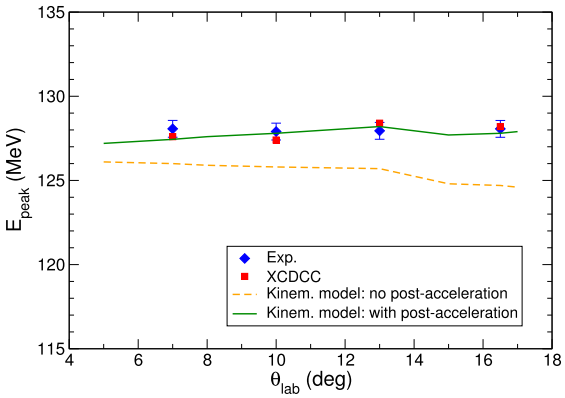

Fig. 7. Position of the centroid of the ^{10}Be energy distributions as a function of the laboratory angle. The experimental peak position (blue diamonds) is compared with the result of the XCDCC calculations (red squares) and with two kinematical calculations, including (solid red line) or excluding (dashed orange line) the effect of post-acceleration effect (see text for details).

The similitude between the CDCC and XCDCC results in Fig. 5 suggests that core excitations are not significant for breakup cross section in the current reaction. This result, which is also consistent with the findings of Refs. [6,10], is interpreted as due to the similar $dB(E1)/dE$ distributions for continuum states predicted by the adopted SP and CEX models. However, it becomes apparent from Fig. 5 that the CDCC and XCDCC calculations fail to reproduce the data for $\theta_{\rm lab} \gtrsim 10°$. Since the (X)CDCC methods account only for the elastic breakup mechanism, we attribute the discrepancy to the presence of nonelastic breakup (NEB) contributions. As in Ref. [6], the latter have been computed using the inclusive-breakup model of Ichimura, Austern and Vincent (IAV) [1], following the implementation performed in Ref. [48]. The calculated ^{10}Be yield arising from NEB is shown by the dashed line in Fig. 5. It is negligible for scattering angles below 10°, but becomes significant above this angle. The sum of the EBU (XCDCC) and NEB contributions (solid green line) agrees rather well with the experimental data.

We notice that the EBU contribution contains both nuclear and Coulomb breakup contributions. With a heavy target, such as the lead target used in this work, the breakup is however expected to be Coulomb dominated. This has been confirmed by performing additional XCDCC calculations retaining all nuclear couplings but only the monopole diagonal Coulomb potential. The result, shown in Fig. 5 by the dotted line, is significantly smaller than the full calculations, where both nuclear and Coulomb couplings are considered, and peaks at larger angles ($\theta_{\rm lab} \sim 12°$).

Further insight on the reaction dynamics could be obtained from the investigation of the energy distributions of the ^{10}Be core, shown in Fig. 6 for the indicated angular intervals. The experimental distributions, corrected by the energy losses in the target and dead-layers of the detectors, are compared with the calculations discussed earlier. For each panel, we show the EBU (XCDCC), NEB (IAV) and their sum (for the lower angular cut, $\theta_{\rm lab} = 6 - 8°$ the NEB contribution is negligible, so it has been omitted for clarity). In general, the sum of the EBU and NEB contributions peak is at about the same ^{10}Be energy and their sum explain rather well the measured distributions, except for some underestimation in the magnitude.

A more detailed inspection of the outgoing energy distribution can shed light on several dynamical aspects of the reaction. In particular, the centroid of the energy distribution and its deviation with respect to simple kinematical considerations provide information on the breakup dynamics [49–51]. Following Ref. [6], we have compared the experimental centroids of the outgoing ^{10}Be energy distributions with those obtained in the XCDCC calculations discussed earlier and with two simple kinematical models. This comparison is shown in Fig. 7. In the first of such models, we assume a binary inelastic-like process with a Q-value given by the optimum excitation energy deduced from the XCDCC calculations. In this model, the final ^{11}Be kinetic energy is determined by the Q-value and the scattering angle. Further, we assume the ^{10}Be kinetic energy is just 10/11 times the energy of the outgoing ^{11}Be. This simple estimate, indicated by the orange arrows in Fig. 6, is found to systematically underpredict the observed ^{10}Be energy peak position. As in [6], we attribute this discrepancy to the post-acceleration experienced by the ^{10}Be fragment in the strong Coulomb field of the high-Z target, following the projectile dissociation. The presence of post-acceleration suggests that (i) the breakup occurs mainly through non-resonant continuum states and (ii) that the breakup takes place in the proximity of the target, where the Coulomb force is strong. Using the arguments given in [6], the additional kinetic energy gained by the charged fragment (^{10}Be) due to the post-acceleration mechanism can be estimated as

$$\Delta E = \frac{m_n}{m_n + m_c} \frac{Z_c Z_t e^2}{R_{\rm bu}}, \qquad (1)$$

where $R_{\rm bu}$ is the projectile-target separation at which the breakup is assumed to take place, $Z_{c,t}$ are the core and target charges and $m_{n,c}$ the neutron and core masses. As in [6], we approximate $R_{\rm bu}$ by the distance of closest approach for the Coulomb trajectory associated to the considered scattering angle. When this extra energy is added to the previous estimate, one obtains the green arrows displayed in Fig. 6. The latter turn out to be in very good agreement with the peak position of the data and the XCDCC calculations, as shown in Fig. 7, reinforcing the importance of the post-acceleration effect and validating the simple kinematical picture. In Fig. 7, the dashed and solid lines correspond to the kinematical estimates without and with post-acceleration, respectively. As can be observed, the calculations including post-acceleration reproduce very well the data.

The sudden fall for $\theta_{\rm lab} \geq 13°$ in the kinematical calculations stems from the fact that, beyond this angle, the optimal excitation energy is associated with the low-lying $5/2^+$ resonance which, in the ^{11}Be model employed in the XCDCC calculations, is located at $E_x \simeq 1.8$ MeV. The XCDCC calculations reproduce also very well the experimental values, which indicates that post-acceleration effects are implicitly taken into account by these calculations, mostly in the form of continuum-continuum couplings.

4. Summary

To summarize, we have presented new quasielastic and breakup data for the ^{11}Be + ^{208}Pb system at an incident energy 3.5 times larger than the Coulomb barrier. Elastic scattering data for the ^{9,10}Be + ^{208}Pb systems were also measured at similar energies. The ^{10}Be elastic data could be well reproduced by optical model calculations using potentials from a global parametrization. The ^{11}Be quasielastic data required an extra long-range absorptive contribution, in agreement with previous studies at near-barrier energies. CDCC and XCDCC calculations, with the later accounting for the effect of the ^{10}Be excitations, have been performed and were found to reproduce quite well the ^{11}Be + ^{208}Pb quasielastic scattering data. The strong suppression of the CNIP in the present ^{11}Be + ^{208}Pb quasi-elastic angular distribution is corroborated by the CDCC and XCDCC calculations. This is somewhat unexpected, insofar as the effects of multistep couplings should decrease with increasing incident energy. The persistence of the strong suppression of the Coulomb-Nuclear interference peak at 3.5 times the Coulomb barrier energy for the neutron-rich halo nucleus ^{11}Be, and not for the proton-rich halo nucleus, such as ^{8}B, is an interesting result that would deserve further investigation.

Comparison of the measured angular and energy distributions of ^{10}Be fragments with the CDCC and XCDCC calculations revealed that these fragments are mostly produced by a EBU mechanism (i.e. elastic dissociation). However, NEB contributions are found to be also present in the data. This contribution has been estimated with the Ichimura-Austern-Vincent model [1]. When added to the EBU contribution, a good account of the data is obtained. A comparison of the measured ^{10}Be outgoing energies with simple kinematical considerations reveals also that these fragments experience a post-acceleration effect after the breakup takes place.

This work suggests that valuable experimental data are still needed to understand the interplay between nuclear structure and reaction mechanisms and to examine the nuclear structure and reaction state-of-the-art theories.

Declaration of competing interest

The authors declare that they have no known competing financial interests or personal relationships that could have appeared to influence the work reported in this paper.

Acknowledgements

We would like to acknowledge the staff of HIRFL for the operation of the cyclotron and those of RIBLL for their friendly collaboration. This work was financially supported by the National Key Research and Development Program of China (Grant No. 2018YFA0404403), the National Natural Science Foundation of China (Grant No. 11775013, No. 11947203, No. 11575256, and No. U1632138) and the Youth Innovation Promotion Association CAS (No. 2020411). A.M.M. is supported by the Spanish Ministerio de Ciencia, Innovación y Universidades and FEDER funds under project FIS2017-88410-P and by the European Union's Horizon 2020 research and innovation program under Grant Agreement No. 654002. V.G. thanks the São Paulo Research Foundation (FAPESP) (Grant No. 2016/17612-7).

References

[1] M. Ichimura, N. Austern, C.M. Vincent, Comparison of approximate formalisms for inclusive breakup reactions, Phys. Rev. C 34 (1986) 2326–2329, https://doi.org/10.1103/PhysRevC.34.2326.

[2] G.R. Satchler, Direct Nuclear Reactions, Clareton, Oxford, 1983.

[3] I. Tanihata, T. Kobayashi, O. Yamakawa, S. Shimoura, K. Ekuni, K. Sugimoto, N. Takahashi, T. Shimoda, H. Sato, Measurement of interaction cross sections using isotope beams of be and b and isospin dependence of the nuclear radii, Phys. Lett. B 206 (4) (1988) 592–596, https://doi.org/10.1016/0370-2693(88)90702-2, http://www.sciencedirect.com/science/article/pii/0370269388907022.

[4] T. Aumann, A. Navin, D.P. Balamuth, D. Bazin, B. Blank, B.A. Brown, J.E. Bush, J.A. Caggiano, B. Davids, T. Glasmacher, V. Guimarães, P.G. Hansen, R.W. Ibbotson, D. Karnes, J.J. Kolata, V. Maddalena, B. Pritychenko, H. Scheit, B.M. Sherrill, J.A. Tostevin, One-neutron knockout from individual single-particle states of ^{11}Be, Phys. Rev. Lett. 84 (2000) 35–38, https://doi.org/10.1103/PhysRevLett.84.35.

[5] J. Chen, J.L. Lou, Y.L. Ye, J. Rangel, A.M. Moro, D.Y. Pang, Z.H. Li, Y.C. Ge, Q.T. Li, J. Li, W. Jiang, Y.L. Sun, H.L. Zang, Y. Zhang, N. Aoi, E. Ideguchi, H.J. Ong, J. Lee, J. Wu, H.N. Liu, C. Wen, Y. Ayyad, K. Hatanaka, T.D. Tran, T. Yamamoto, M. Tanaka, T. Suzuki, T.T. Nguyen, Elastic scattering and breakup of ^{11}Be on deuterons at 26.9*A* MeV, Phys. Rev. C 94 (2016) 064620, https://doi.org/10.1103/PhysRevC.94.064620.

[6] A.D. Pietro, A. Moro, J. Lei, R. de Diego, Insights into the dynamics of breakup of the halo nucleus ^{11}Be on a ^{64}Zn target, Phys. Lett. B 798 (2019) 134954, https://doi.org/10.1016/j.physletb.2019.134954, http://www.sciencedirect.com/science/article/pii/S0370269319306768.

[7] A. Di Pietro, G. Randisi, V. Scuderi, L. Acosta, F. Amorini, M.J.G. Borge, P. Figuera, M. Fisichella, L.M. Fraile, J. Gomez-Camacho, H. Jeppesen, M. Lattuada, I. Martel, M. Milin, A. Musumarra, M. Papa, M.G. Pellegriti, F. Perez-Bernal, R. Raabe, F. Rizzo, D. Santonocito, G. Scalia, O. Tengblad, D. Torresi, A.M. Vidal, D. Voulot, F. Wenander, M. Zadro, Elastic scattering and reaction mechanisms of the halo nucleus ^{11}Be around the Coulomb barrier, Phys. Rev. Lett. 105 (2010) 022701, https://doi.org/10.1103/PhysRevLett.105.022701.

[8] A. Di Pietro, V. Scuderi, A.M. Moro, L. Acosta, F. Amorini, M.J.G. Borge, P. Figuera, M. Fisichella, L.M. Fraile, J. Gomez-Camacho, H. Jeppesen, M. Lattuada, I. Martel, M. Milin, A. Musumarra, M. Papa, M.G. Pellegriti, F. Perez-Bernal, R. Raabe, G. Randisi, F. Rizzo, G. Scalia, O. Tengblad, D. Torresi, A.M. Vidal, D. Voulot, F. Wenander, M. Zadro, Experimental study of the collision ^{11}Be+^{64}Zn around the Coulomb barrier, Phys. Rev. C 85 (2012) 054607, https://doi.org/10.1103/PhysRevC.85.054607.

[9] L. Acosta, M.A.G. Álvarez, M.V. Andrés, M.J.G. Borge, M. Cortés, J.M. Espino, D. Galaviz, J. Gómez-Camacho, A. Maira, I. Martel, A.M. Moro, I. Mukha, F. Pérez-Bernal, E. Reillo, D. Rodríguez, K. Rusek, A.M. Sánchez-Benítez, O. Tengblad, Signature of a strong coupling with the continuum in ^{11}Be +^{120} Sn scattering at the Coulomb barrier, Eur. Phys. J. A 42 (3) (2009) 461, https://doi.org/10.1140/epja/i2009-10822-6.

[10] V. Pesudo, M.J.G. Borge, A.M. Moro, J.A. Lay, E. Nácher, J. Gómez-Camacho, O. Tengblad, L. Acosta, M. Alcorta, M.A.G. Alvarez, C. Andreoiu, P.C. Bender, R. Braid, M. Cubero, A. Di Pietro, J.P. Fernández-García, P. Figuera, M. Fisichella, B.R. Fulton, A.B. Garnsworthy, G. Hackman, U. Hager, O.S. Kirsebom, K. Kuhn, M. Lattuada, G. Marquínez-Durán, I. Martel, D. Miller, M. Moukaddam, P.D. O'-Malley, A. Perea, M.M. Rajabali, A.M. Sánchez-Benítez, F. Sarazin, V. Scuderi, C.E. Svensson, C. Unsworth, Z.M. Wang, Scattering of the halo nucleus ^{11}Be on ^{197}Au at energies around the Coulomb barrier, Phys. Rev. Lett. 118 (2017) 152502, https://doi.org/10.1103/PhysRevLett.118.152502.

[11] M. Mazzocco, C. Signorini, M. Romoli, A. De Francesco, M. Di Pietro, E. Vardaci, K. Yoshida, A. Yoshida, R. Bonetti, A. De Rosa, T. Glodariu, A. Guglielmetti, G. Inglima, M. La Commara, B. Martin, D. Pierroutsakou, F. Sandoli, M. nd Soramel, L. Stroe, N. Kanungo, R. nd Khai, T. Motobayashi, T. Nomura, T. Ishikawa, H. Ishiyama, S. Jeong, H. Miyatake, M.H. Tanaka, I. Sugai, Y. Watanabe, Scattering of ^{11}Be halo nucleus from ^{209}Bi at the Coulomb barrier, Eur. Phys. J. A 28 (3) (2006) 295–299, https://doi.org/10.1140/epja/i2006-10058-0.

[12] M. Mazzocco, C. Signorini, M. Romoli, R. Bonetti, A. De Francesco, A. De Rosa, M. Di Pietro, L. Fortunato, T. Glodariu, A. Guglielmetti, G. Inglima, T. Ishikawa, H. Ishiyama, R. Kanungo, N. Khai, S. Jeong, M. La Commara, B. Martin, H. Miyatake, T. Motobayashi, T. Nomura, D. Pierroutsakou, M. Sandoli, F. Soramel, L. Stroe, I. Sugai, M.H. Tanaka, E. Vardaci, Y. Watanabe, A. Yoshida, K. Yoshida, Elastic scattering for the system ^{11}Be +^{209} Bi at Coulomb barrier energies, Eur. Phys. J. Spec. Top. 150 (1) (2007) 37–40, https://doi.org/10.1140/epjst/e2007-00260-2.

[13] E.F. Aguilera, J.J. Kolata, F.M. Nunes, F.D. Becchetti, P.A. DeYoung, M. Goupell, V. Guimarães, B. Hughey, M.Y. Lee, D. Lizcano, E. Martinez-Quiroz, A. Nowlin, T.W. O'Donnell, G.F. Peaslee, D. Peterson, P. Santi, R. White-Stevens, Transfer and/or breakup modes in the ^{6}He+^{209}Bi reaction near the Coulomb barrier, Phys. Rev. Lett. 84 (2000) 5058–5061, https://doi.org/10.1103/PhysRevLett.84.5058.

[14] O. Kakuee, J. Rahighi, A. Sánchez-Benítez, M. Andrés, S. Cherubini, T. Davinson, W. Galster, J. Gómez-Camacho, A. Laird, M. Lamehi-Rachti, I. Martel, A. Shotter, W. Smith, J. Vervier, P. Woods, Elastic scattering of the halo nucleus ^{6}He from ^{208}Pb above the Coulomb barrier, Nucl. Phys. A 728 (3) (2003) 339–349, https://doi.org/10.1016/j.nuclphysa.2003.08.030, http://www.sciencedirect.com/science/article/pii/S0375947403017329.

[15] A. Di Pietro, P. Figuera, F. Amorini, C. Angulo, G. Cardella, S. Cherubini, T. Davinson, D. Leanza, J. Lu, H. Mahmud, M. Milin, A. Musumarra, A. Ninane, M. Papa, M.G. Pellegriti, R. Raabe, F. Rizzo, C. Ruiz, A.C. Shotter, N. Soić, S. Tudisco, L. Weissman, Reactions induced by the halo nucleus ^{6}He at energies around the Coulomb barrier, Phys. Rev. C 69 (2004) 044613, https://doi.org/10.1103/PhysRevC.69.044613.

[16] A.M. Moro, K. Rusek, J.M. Arias, J. Gómez-Camacho, M. Rodríguez-Gallardo, Improved di-neutron cluster model for ^{6}He scattering, Phys. Rev. C 75 (2007) 064607, https://doi.org/10.1103/PhysRevC.75.064607.

[17] L. Acosta, A.M. Sánchez-Benítez, M.E. Gómez, I. Martel, F. Pérez-Bernal, F. Pizarro, J. Rodríguez-Quintero, K. Rusek, M.A.G. Alvarez, M.V. Andrés, J.M. Espino, J.P. Fernández-García, J. Gómez-Camacho, A.M. Moro, C. Angulo, J. Cabrera, E. Casarejos, P. Demaret, M.J.G. Borge, D. Escrig, O. Tengblad, S. Cherubini, P. Figuera, M. Gulino, M. Freer, C. Metelko, V. Ziman, R. Raabe, I. Mukha, D. Smirnov, O.R. Kakuee, J. Rahighi, Elastic scattering and α-particle production in ^{6}He + ^{208}Pb collisions at 22 MeV, Phys. Rev. C 84 (2011) 044604, https://doi.org/10.1103/PhysRevC.84.044604.

[18] M. Cubero, J.P. Fernández-García, M. Rodríguez-Gallardo, L. Acosta, M. Alcorta, M.A.G. Alvarez, M.J.G. Borge, L. Buchmann, C.A. Diget, H.A. Falou, B.R. Fulton, H.O.U. Fynbo, D. Galaviz, J. Gómez-Camacho, R. Kanungo, J.A. Lay, M. Madurga, I. Martel, A.M. Moro, I. Mukha, T. Nilsson, A.M. Sánchez-Benítez, A. Shotter, O. Tengblad, P. Walden, Do halo nuclei follow Rutherford elastic scattering at energies below the barrier? The case of ^{11}Li, Phys. Rev. Lett. 109 (2012) 262701, https://doi.org/10.1103/PhysRevLett.109.262701.

[19] E.F. Aguilera, E. Martinez-Quiroz, D. Lizcano, A. Gómez-Camacho, J.J. Kolata, L.O. Lamm, V. Guimarães, R. Lichtenthäler, O. Camargo, F.D. Becchetti, H. Jiang, P.A. DeYoung, P.J. Mears, T.L. Belyaeva, Reaction cross sections for ^{8}B, ^{7}Be, and ^{6}Li + ^{58}Ni near the Coulomb barrier: proton-halo effects, Phys. Rev. C 79 (2009) 021601, https://doi.org/10.1103/PhysRevC.79.021601.

[20] M. Mazzocco, N. Keeley, A. Boiano, C. Boiano, M. La Commara, C. Manea, C. Parascandolo, D. Pierroutsakou, C. Signorini, E. Strano, D. Torresi, H. Yamaguchi, D. Kahl, L. Acosta, P. Di Meo, J.P. Fernandez-Garcia, T. Glodariu, J. Grebosz, A. Guglielmetti, Y. Hirayama, N. Imai, H. Ishiyama, N. Iwasa, S.C. Jeong, H.M. Jia, Y.H. Kim, S. Kimura, S. Kubono, G. La Rana, C.J. Lin, P. Lotti, G. Marquínez-Durán, I. Martel, H. Miyatake, M. Mukai, T. Nakao, M. Nicoletto, A. Pakou, K. Rusek, Y. Sakaguchi, A.M. Sánchez-Benítez, T. Sava, O. Sgouros, V. Soukeras, F. Soramel, E. Stiliaris, L. Stroe, T. Teranishi, N. Toniolo, Y. Wakabayashi, Y.X. Watanabe, L. Yang, Y.Y. Yang, H.Q. Zhang, Elastic scattering for the ^{8}B and ^{7}Be + ^{208}Pb systems at near-Coulomb barrier energies, Phys. Rev. C 100 (2019) 024602, https://doi.org/10.1103/PhysRevC.100.024602.

[21] Y.Y. Yang, J.S. Wang, Q. Wang, D. Pang, J.B. Ma, M.R. Huang, J.L. Han, P. Ma, S.L. Jin, Z. Bai, Q. Hu, L. Jin, J.B. Chen, N. Keeley, K. Rusek, R. Wada, S. Mukherjee, Z.Y. Sun, R.F. Chen, X.Y. Zhang, Z.G. Hu, X.H. Yuan, X.G. Cao, Z.G. Xu, S.W. Xu, C. Zhen, Z.Q. Chen, Z. Chen, S.Z. Chen, C.M. Du, L.M. Duan, F. Fu, B.X. Gou, J. Hu, J.J. He, X.G. Lei, S.L. Li, Y. Li, Q.Y. Lin, L.X. Liu, F.D. Shi, S.W. Tang, G. Xu, X. Xu, L.Y. Zhang, X.H. Zhang, W. Zhang, M.H. Zhao, Z.Y. Guo, Y.H. Zhang, H.S. Xu, G.Q. Xiao, Elastic scattering of the proton drip-line nucleus ^{8}B off a ^{nat}Pb target at 170.3 MeV, Phys. Rev. C 87 (2013) 044613, https://doi.org/10.1103/PhysRevC.87.044613.

[22] Y.Y. Yang, J.S. Wang, Q. Wang, D.Y. Pang, J.B. Ma, M.R. Huang, P. Ma, S.L. Jin, J.L. Han, Z. Bai, L. Jin, J.B. Chen, Q. Hu, R. Wada, S. Mukherjee, Z.Y. Sun, R.F. Chen, X.Y. Zhang, Z.G. Hu, X.H. Yuan, S.W. Xu, S.Z. Chen, X.G. Lei, L.X. Liu, W.H. Ma, S.T. Wang, D. Yan, X.H. Zhang, M.H. Zhao, Y. Zhou, Y.J. Zhou, Z.Y. Guo, Y.H. Zhang, H.S. Xu, G.Q. Xiao, Quasi-elastic scattering of ^{10,11}C and ^{10}B from a ^{nat}Pb target, Phys. Rev. C 90 (2014) 014606, https://doi.org/10.1103/PhysRevC.90.014606.

[23] Y.Y. Yang, X. Liu, D.Y. Pang, D. Patel, R.F. Chen, J.S. Wang, P. Ma, J.B. Ma, S.L. Jin, Z. Bai, V. Guimarães, Q. Wang, W.H. Ma, F.F. Duan, Z.H. Gao, Y.C. Yu, Z.Y. Sun, Z.G. Hu, S.W. Xu, S.T. Wang, D. Yan, Y. Zhou, Y.H. Zhang, X.H. Zhou, H.S. Xu, G.Q. Xiao, W.L. Zhan, Elastic scattering of the proton drip line nuclei ^{7}Be,^{8}B, and ^{9}C on a lead target at energies around three times the Coulomb barriers, Phys. Rev. C 98 (2018) 044608, https://doi.org/10.1103/PhysRevC.98.044608.

[24] J.F. Liang, J.R. Beene, H. Esbensen, A. Galindo-Uribarri, J. Gomez del Campo, C.J. Gross, M.L. Halbert, P.E. Mueller, D. Shapira, D.W. Stracener, I.J. Thompson, R.L. Varner, Elastic scattering and breakup of ^{17}F at 10 MeV/nucleon, Phys. Rev. C 65 (2002) 051603, https://doi.org/10.1103/PhysRevC.65.051603.

[25] J.F. Liang, J.R. Beene, A. Galindo-Uribarri, J. Gomez del Campo, C.J. Gross, P.A. Hausladen, P.E. Mueller, D. Shapira, D.W. Stracener, R.L. Varner, J.D. Bierman, H. Esbensen, Y. Larochelle, Breakup of ^{17}F on ^{208}Pb near the Coulomb barrier, Phys. Rev. C 67 (2003) 044603, https://doi.org/10.1103/PhysRevC.67.044603.

[26] M. Romoli, E. Vardaci, M. Di Pietro, A. De Francesco, A. De Rosa, G. Inglima, M. La Commara, B. Martin, D. Pierroutsakou, M. Sandoli, M. Mazzocco, T. Glodariu, P. Scopel, C. Signorini, R. Bonetti, A. Guglielmetti, F. Soramel, L. Stroe, J. Greene, A. Heinz, D. Henderson, C.L. Jiang, E.F. Moore, R.C. Pardo, K.E. Rehm, A. Wuosmaa, J.F. Liang, Measurements of ^{17}F scattering by ^{208}Pb with a new type of large solid angle detector array, Phys. Rev. C 69 (2004) 064614, https://doi.org/10.1103/PhysRevC.69.064614.

[27] N. Keeley, N. Alamanos, K. Kemper, K. Rusek, Elastic scattering and reactions of light exotic beams, Prog. Part. Nucl. Phys. 63 (2) (2009) 396–447, https://doi.org/10.1016/j.ppnp.2009.05.003, http://www.sciencedirect.com/science/article/pii/S0146641009000519.

[28] J. Lubian, T. Correa, E.F. Aguilera, L.F. Canto, A. Gomez-Camacho, E.M. Quiroz, P.R.S. Gomes, Effects of breakup couplings on ^{8}B + ^{58}Ni elastic scattering, Phys. Rev. C 79 (2009) 064605, https://doi.org/10.1103/PhysRevC.79.064605.

[29] N. Keeley, Elastic scattering a hundred years on what can it tell us?, J. Phys. Conf. Ser. 381 (2012) 012087, https://doi.org/10.1088/1742-6596/381/1/012087.

[30] P. Descouvemont, E.C. Pinilla, Microscopic description of ^{8}Li + nucleus and of ^{8}B + nucleus scattering, Few-Body Syst. 60 (1) (2018) 11, https://doi.org/10.1007/s00601-018-1476-6.

[31] Y.Y. Yang, X. Liu, D.Y. Pang, Distinction between elastic scattering of weakly bound proton- and neutron-rich nuclei: the case of ^{8}B and ^{11}Be, Phys. Rev. C 94 (2016) 034614, https://doi.org/10.1103/PhysRevC.94.034614.

[32] Z. Sun, W.-L. Zhan, Z.-Y. Guo, G. Xiao, J.-X. Li, RIBLL, the radioactive ion beam line in Lanzhou, Nucl. Instrum. Methods Phys. Res., Sect. A, Accel. Spectrom. Detect. Assoc. Equip. 503 (3) (2003) 496–503, https://doi.org/10.1016/S0168-9002(03)01005-2, http://www.sciencedirect.com/science/article/pii/S0168900203010052.

[33] J. Xia, W. Zhan, B. Wei, Y. Yuan, M. Song, W. Zhang, X. Yang, P. Yuan, D. Gao, H. Zhao, X. Yang, G. Xiao, K. Man, J. Dang, X. Cai, Y. Wang, J. Tang, W. Qiao, Y. Rao, Y. He, L. Mao, Z. Zhou, The heavy ion cooler-storage-ring project (HIRFL-CSR) at Lanzhou, Nucl. Instrum. Methods Phys. Res., Sect. A, Accel. Spectrom. Detect. Assoc. Equip. 488 (1) (2002) 11–25, https://doi.org/10.1016/S0168-9002(02)00475-8, http://www.sciencedirect.com/science/article/pii/S0168900202004758.

[34] Y. Yang, J. Wang, Q. Wang, J. Ma, M. Huang, J. Han, P. Ma, S. Jin, Z. Bai, Q. Hu, L. Jin, J. Chen, R. Wada, Z. Sun, R. Chen, X. Zhang, Z. Hu, X. Yuan, X. Cao, Z. Xu, S. Xu, C. Zhen, Z. Chen, Z. Chen, S. Chen, C. Du, L. Duan, F. Fu, B. Gou, J. Hu, J. He, X. Lei, S. Li, Y. Li, Q. Lin, L. Liu, F. Shi, S. Tang, G. Xu, X. Xu, L. Zhang, X. Zhang, W. Zhang, M. Zhao, Y. Zhang, H. Xu, A method for the measurement of elastic scattering angular distribution at HIRFL-RIBLL, Nucl. Instrum. Methods Phys. Res., Sect. A, Accel. Spectrom. Detect. Assoc. Equip. 701 (2013) 1–6, https://doi.org/10.1016/j.nima.2012.10.088, http://www.sciencedirect.com/science/article/pii/S0168900212012569.

[35] F.-F. Duan, Y.-Y. Yang, D.-Y. Pang, B.-T. Hu, J.-S. Wang, K. Wang, G. Yang, V. Guimarães, P. Ma, S.-W. Xu, X.-Q. Liu, J.-B. Ma, Z. Bai, Q. Hu, S.-Y. Jin, X.-X. Sun, J.-S. Yao, H.-K. Qi, Z.-Y. Sun, Experimental study of the elastic scattering of ^{10}Be on ^{208}Pb at the energy of around three times the Coulomb barrier, Chin. Phys. C 44 (2) (2020) 024001, https://doi.org/10.1088/1674-1137/44/2/024001.

[36] Y.P. Xu, D.Y. Pang, Toward a systematic nucleus-nucleus potential for peripheral collisions, Phys. Rev. C 87 (2013) 044605, https://doi.org/10.1103/PhysRevC.87.044605.

[37] M. Andrés, J. Gómez-Camacho, M. Nagarajan, Dynamic polarization potential induced by dipole Coulomb excitation, Nucl. Phys. A 579 (1) (1994) 273–284, https://doi.org/10.1016/0375-9474(94)90806-0, http://www.sciencedirect.com/science/article/pii/0375947494908060.

[38] M. Andrés, J. Gómez-Camacho, M. Nagarajan, Dynamic polarization potential induced by dipole Coulomb excitation to break-up states in ^{11}Li scattering, Nucl. Phys. A 583 (1995) 817–820, https://doi.org/10.1016/0375-9474(94)00765-F, nucleus-Nucleus Collisions, http://www.sciencedirect.com/science/article/pii/037594749400765F.

[39] W.Y. So, K.S. Kim, K.S. Choi, M.-K. Cheoun, Long-range dynamic polarization potentials for ^{11}Be projectiles on ^{64}Zn, Phys. Rev. C 92 (2015) 014627, https://doi.org/10.1103/PhysRevC.92.014627.

[40] T. Tarutina, L.C. Chamon, M.S. Hussein, Coulomb excitation of ^{11}Be reexamined, Phys. Rev. C 67 (2003) 044605, https://doi.org/10.1103/PhysRevC.67.044605.

[41] N. Fukuda, T. Nakamura, N. Aoi, N. Imai, M. Ishihara, T. Kobayashi, H. Iwasaki, T. Kubo, A. Mengoni, M. Notani, H. Otsu, H. Sakurai, S. Shimoura, T. Teranishi, Y.X. Watanabe, K. Yoneda, Coulomb and nuclear breakup of a halo nucleus ^{11}Be, Phys. Rev. C 70 (2004) 054606, https://doi.org/10.1103/PhysRevC.70.054606.

[42] P. Capel, F.M. Nunes, Influence of the projectile description on breakup calculations, Phys. Rev. C 73 (2006) 014615, https://doi.org/10.1103/PhysRevC.73.014615.

[43] F. Nunes, J. Christley, I. Thompson, R. Johnson, V. Efros, Core excitation in three-body systems: application to ^{12}Be, Nucl. Phys. A 609 (1) (1996) 43–73, https://doi.org/10.1016/0375-9474(96)00284-9, http://www.sciencedirect.com/science/article/pii/0375947496002849.

[44] R. de Diego, J.M. Arias, J.A. Lay, A.M. Moro, Continuum-discretized coupled-channels calculations with core excitation, Phys. Rev. C 89 (2014) 064609, https://doi.org/10.1103/PhysRevC.89.064609.

[45] S. Karataglidis, K. Amos, B.G. Giraud, Local scale transformations and extended matter distributions in nuclei, Phys. Rev. C 71 (2005) 064601.

[46] J.A. Lay, A.M. Moro, J.M. Arias, J. Gómez-Camacho, Particle motion in a deformed potential using a transformed oscillator basis, Phys. Rev. C 85 (2012) 054618, https://doi.org/10.1103/PhysRevC.85.054618.

[47] A. Koning, J. Delaroche, Local and global nucleon optical models from 1 keV to 200 MeV, Nucl. Phys. A 713 (3) (2003) 231–310, https://doi.org/10.1016/S0375-9474(02)01321-0, http://www.sciencedirect.com/science/article/pii/S0375947402013210.

[48] J. Lei, A.M. Moro, Reexamining closed-form formulae for inclusive breakup: application to deuteron- and ^{6}Li-induced reactions, Phys. Rev. C 92 (2015) 044616, https://doi.org/10.1103/PhysRevC.92.044616.

[49] T. Nakamura, S. Shimoura, T. Kobayashi, T. Teranishi, K. Abe, N. Aoi, Y. Doki, M. Fujimaki, N. Inabe, N. Iwasa, K. Katori, T. Kubo, H. Okuno, T. Suzuki, I. Tanihata, Y. Watanabe, A. Yoshida, M. Ishihara, Coulomb dissociation of a halo nucleus ^{11}Be at 72A MeV, Phys. Lett. B 331 (3) (1994) 296–301, https://doi.org/10.1016/0370-2693(94)91055-3, http://www.sciencedirect.com/science/article/pii/0370269394910553.

[50] K. Ieki, D. Sackett, A. Galonsky, C.A. Bertulani, J.J. Kruse, W.G. Lynch, D.J. Morrissey, N.A. Orr, H. Schulz, B.M. Sherrill, A. Sustich, J.A. Winger, F. Deák, A. Horváth, A. Kiss, Z. Seres, J.J. Kolata, R.E. Warner, D.L. Humphrey, Coulomb dissociation of ^{11}Li, Phys. Rev. Lett. 70 (1993) 730–733, https://doi.org/10.1103/PhysRevLett.70.730.

[51] D. Sackett, K. Ieki, A. Galonsky, C.A. Bertulani, H. Esbensen, J.J. Kruse, W.G. Lynch, D.J. Morrissey, N.A. Orr, B.M. Sherrill, H. Schulz, A. Sustich, J.A. Winger, F. Deák, A. Horváth, A. Kiss, Z. Seres, J.J. Kolata, R.E. Warner, D.L. Humphrey, Electromagnetic excitation of ^{11}Li, Phys. Rev. C 48 (1993) 118–135, https://doi.org/10.1103/PhysRevC.48.118.